Electronic Supplementary Material (ESI) for Inorganic Chemistry Frontiers.
This journal is © the Partner Organisations 2022

Supporting Information

Tuning Excited States Energy Levels through Achieving Coordination Induced Thermally Activated Delayed Fluorescence

*Dong Liang, Ji-Hui Jia, Xian-Bao Cai, Yu-Qing Zhao, Zhan-Qi Wang, Can-Zhong Lu**

Contents

1. Materials and Instruments

^{1}H NMR and ^{13}C NMR spectra were recorded on a Bruker Avance III 400 MHz NMR spectrometer and a JEOL ECZ400S 400 MHz NMR spectrometer for CD_2Cl_2. Chemical shifts were given in ppm referenced to tetramethylsilane (TMS, $\delta = 0$ ppm). Peak multiplicities were reported with the notation s (singlet), d (double), t (triplet), q (quartet), and m (multiplet). Elemental analyses (C, H, C) were implemented with an Elementary Vario EL III elemental analyzer. Thermogravimetric analyses (TGA) of samples were performed on METTLER TOLEDO TGA/DSC 1 STARe System with a heating rate of 10°C/min under nitrogen. At a scan rate of 5° min^{-1} (scan range: 5° - 60°).

All UV-visible absorption spectra were determined on a PerkinElmer Lambda 650 spectrophotometer under ambient conditions. Steady-state photoluminescence spectra at 298 K were measured using Edinburgh Analytical instrument FLS980. Photoluminescence spectra at 77K and time-resolved photoluminescent decay experiments (lifetime) were performed on an Edinburgh Analytical instrument LP980 equipped with OPO laser and FLS980 equipped with both xenon arc lamp (450 W) and pulsed flash lamps. Delayed emission spectra in solution recorded by Edinburgh Analytical instrument FLS980 equipped with EPL-375 laser. The variable-temperature measurements were carried out on corresponding instruments by using an additional LINKAM THMS600 system. 10wt% doped PMMA films were fabricated by spin-coating DCM solution with concentration of 20mg/ml.

2. Synthesis of Materials

Synthesis of Complexes **1** and **2**. A mixture of $[Ag(CH_3CN)_4]BF_4$ and corresponding phosphine ligand (1 mmol POP or Xantphos) in CH_2Cl_2 (5 mL) was stirred for 20 min at room temperature, and then spiro-2N (1 mmol) was added. After the mixture was stirred for another 2 hours, the solvent was removed by evaporation. Single crystals of these two complexes suitable for X-ray diffraction measurements were obtained by diffusion of ether into CH_2Cl_2 solution.

[Ag(spiro-2N)(POP)]BF_4 (**1**). ^{1}H NMR (400 MHz, Methylene Chloride-d_2) δ 8.58 (d, J = 18.9 Hz, 2H), 7.96 (d, J = 8.9 Hz, 2H), 7.75 (t, J = 7.7 Hz, 2H), 7.63 (t, J = 7.7 Hz, 1H), 7.52 – 7.45 (m, 4H), 7.43 – 7.35 (m, 4H), 7.30 (p, J = 8.0, 7.3 Hz, 18H), 7.02 (d, J = 7.0 Hz, 3H), 6.93 (t, J = 7.6 Hz, 1H), 6.85 (d, J = 3.8 Hz, 4H), 6.62 – 6.56 (m, 2H), 6.43 (d, J = 8.5 Hz, 2H), 6.18 (d, J = 13.1 Hz, 2H). ^{13}C NMR (101 MHz, Methylene Chloride-d_2) δ 157.52, 142.17, 140.68, 134.67, 134.29, 134.19, 132.61, 131.87, 131.29, 131.14, 130.54, 129.60, 129.56, 129.51, 129.12, 127.22, 127.08, 125.27, 123.93, 121.48, 119.25, 116.12.

[Ag(spiro-2N)(XANT)]BF_4 (**2**). ^{1}H NMR (400 MHz, Methylene Chloride-d_2) δ 8.53 (d, J = 4.9 Hz, 2H), 7.99 (d, J = 7.7 Hz, 2H), 7.76 (t, J = 8.0 Hz, 2H), 7.69 (d, J = 7.8 Hz, 2H), 7.67 – 7.60 (m, 1H), 7.50 (dd, J = 12.6, 6.0 Hz, 4H), 7.39 – 7.31 (m, 4H), 7.29 – 7.13 (m, 18H), 7.03 (t, J = 7.8 Hz, 2H), 6.68 (dt, J = 6.3, 4.0 Hz, 2H), 6.61 (t, J = 7.5 Hz, 2H), 6.45 (d, J = 8.4 Hz, 2H), 6.20 (d, J = 7.8 Hz, 2H), 1.89 (s, 6H). ^{13}C NMR (101 MHz, Methylene Chloride-d_2) δ 151.15, 149.44, 141.65, 140.17, 135.55, 133.42, 133.33, 133.24, 132.60, 131.83, 131.32, 130.74, 130.39, 129.82, 128.98, 128.95, 128.90, 128.85, 128.55, 128.01, 126.58, 126.51, 124.78, 120.97, 119.99, 115.60, 35.29, 29.51.

3. NMR Spectra

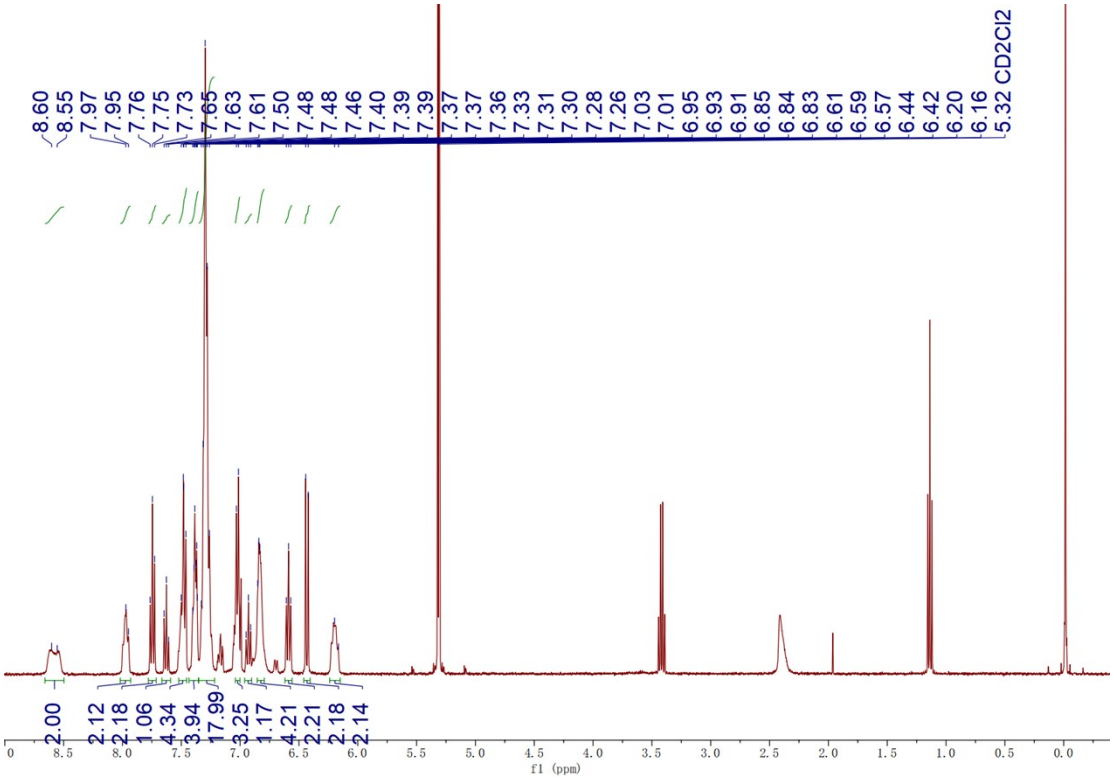

Fig. S1. ^{1}H NMR spectrum of **1**.

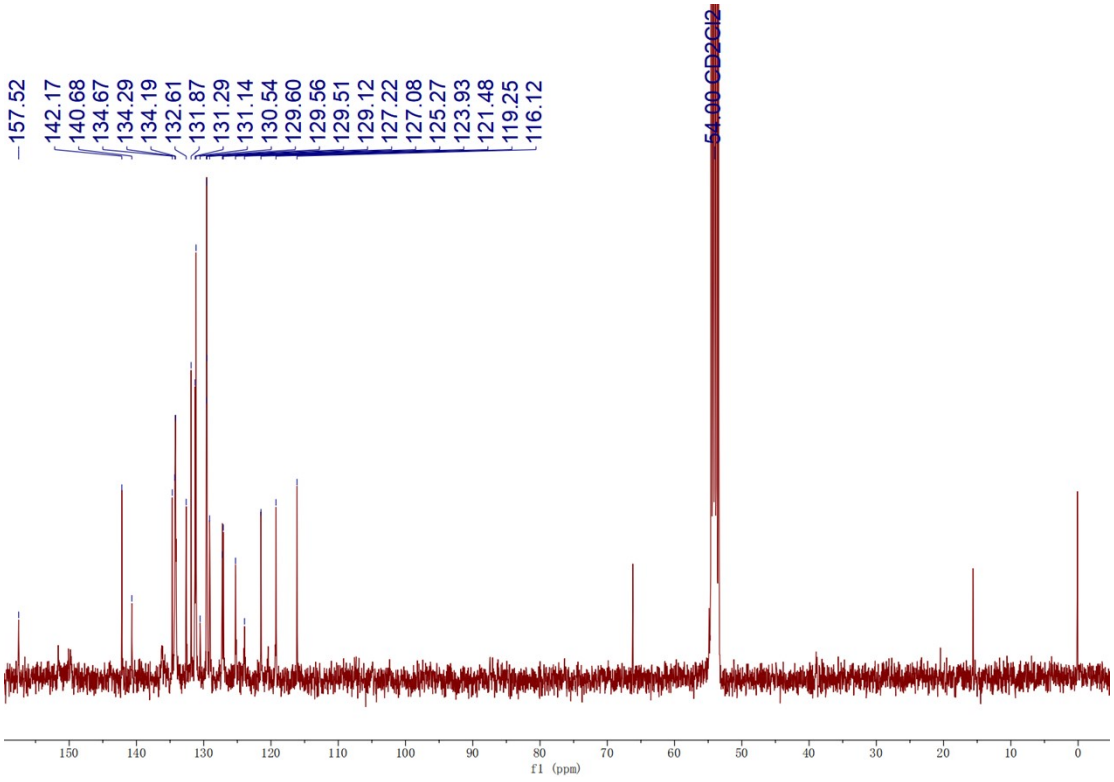

Fig. S2. ^{13}C NMR spectrum of **1**.

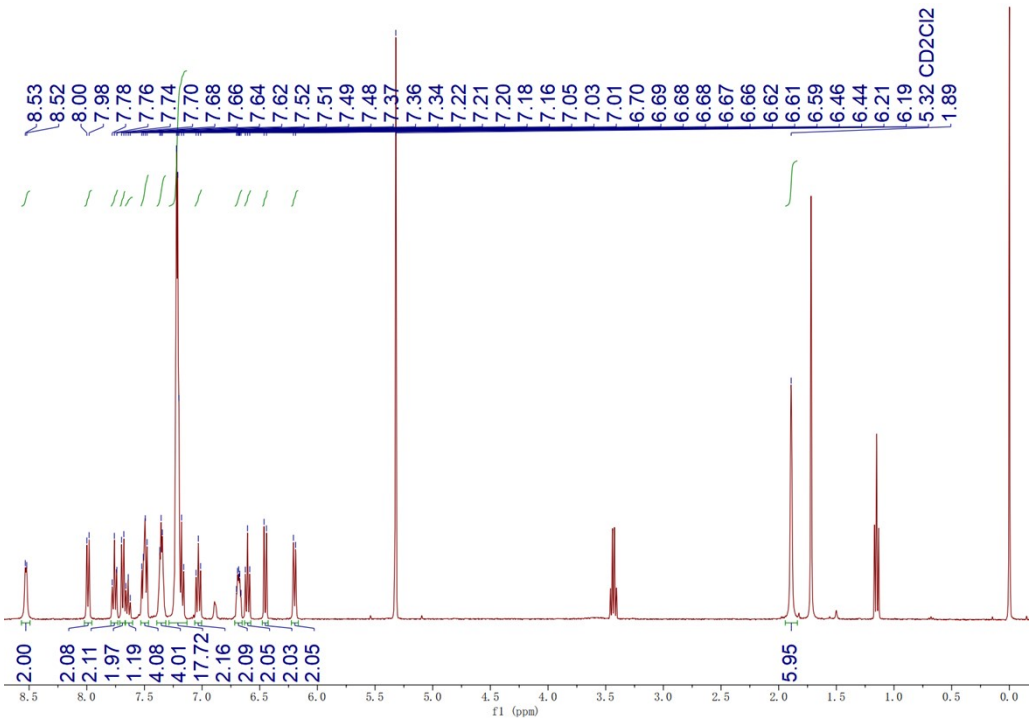

Fig. S3. ^{1}H NMR spectrum of **2**.

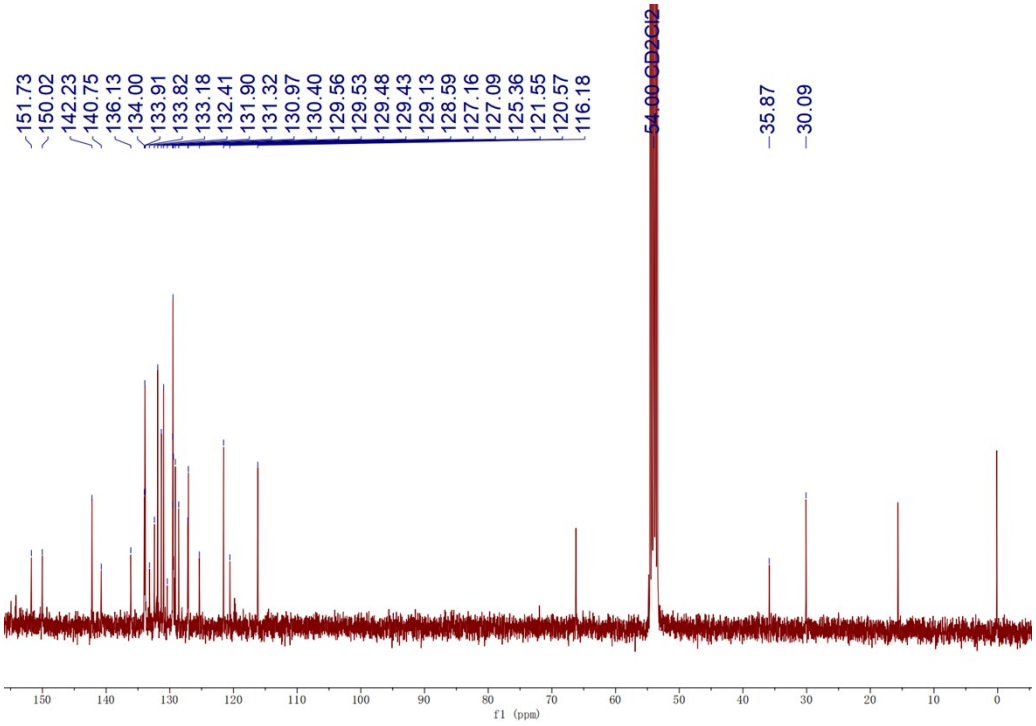

Fig. S4. ^{13}C NMR spectrum of **2**.

4. Thermogravimetric Analysis

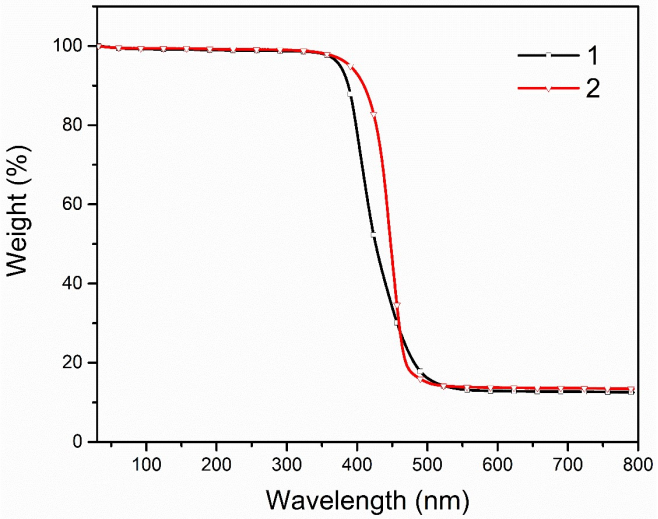

Fig. S5. TGA curves of **1** and **2**.

5. Electrochemical measurements.

Cyclic voltammetry was performed in a gastight single-compartment three-electrode cell with a CHI604E Voltammetric Analyzer at room temperature. A glassy carbon disk and a platinum wire were selected as the working and auxiliary electrodes, respectively. The reference electrode was Ag/Ag+ (0.01 M of AgNO3 in acetonitrile). The CV measurements were carried out in anhydrous and nitrogen-saturated acetonitrile solutions with 0.1 M n-tetrabutylammonium hexafluorophosphate and 2.0 mM investigated compounds. The ferrocenium/ferrocene couple was used as an internal standard.

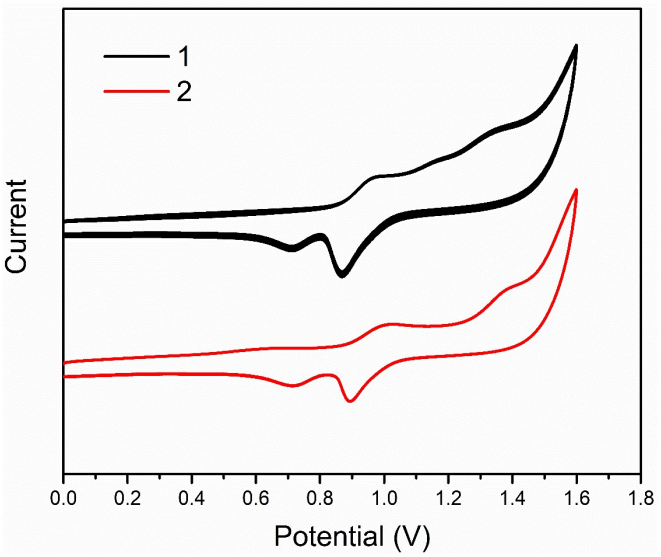

Fig. S6. Cyclic voltammogram of compound **1** and **2** in degassed Dichloromethane.

6. X-ray Crystallographic Analysis

The crystalline samples of the two complexes were obtained from the slow evaporation of the mixture solution of ethyl alcohol and dichloromethane. Diffraction data of the complexes (1 and 2) were collected on a SuperNova, Dual, Cu at zero, Atlas diffractometer equipped with graphite-monochromated Cu Kα radiation (λ = 1.54184 Å). Crystallographic data for this paper are recorded in Cambridge Crystallographic Data Centre (CCDC) with numbers: 2193543 and 2193544. These data can be obtained free of charge from the CCDC via www.ccdc.cam.ac.uk/data_request/cif. The crystalline structure and data of compound spiro-2N reference to the literature [1].

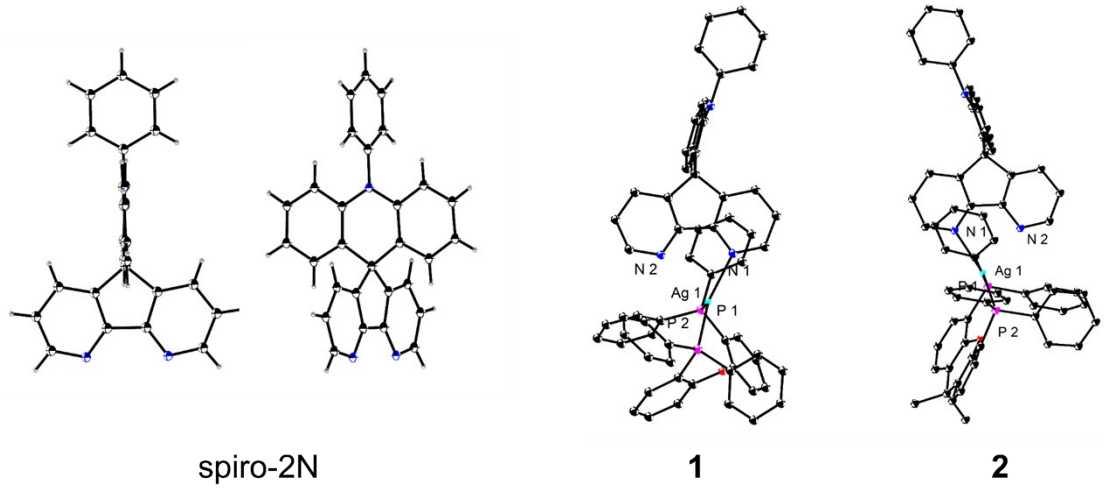

Fig. S7. X-ray structures of ligand spiro-2N and complex **1** and **2**.

Table S1. Crystal data for **1** and **2**.

Sample name	**1**	**2**
Chemical formula	$C_{65}H_{47}AgBF_4N_3OP_2$	$C_{69}H_{53}AgBCl_2F_4N_3OP_2$
Formula weight	1142.67 g/mol	1267.66 g/mol
Crystal system	monoclinic	monoclinic
Space group	$P2_1/n$	$P2_1/c$
a/Å	9.3165(2)	9.4588(3)
b/Å	26.4496(7)	23.6320(8)
c/Å	24.4831(6)	28.8210(8)
α/°	90	90
β/°	96.443(2)	97.142(3)
γ/°	90	90
Volume/Å^3	5994.96(30)	6392.38(30)
Z	4	4
ρ_{calc}g/cm^3	1.26595	1.31711
μ/mm^{-1}	3.649	4.226
Temperature/K	124(30)	99.9(4)
R_{int}	0.0588	0.0408
Goodness-of-fit on F^2	2336	2592
R_1[I>=2σ(I)]	0.0803	0.0673

$wR_2[I>=2\sigma(I)]$	0.2869	0.1830

Table S2. Selected bond distances (Å) and angles (º) of complexes **1** and **2**.

Compound		**1**	**2**
Distances(Å)	Ag1-N1	2.283(5)	2.333(3)
	Ag1-P1	2.5046(18)	2.4346(10)
	Ag1-P2	2.4237(17)	2.4827(11)
	Ag1-N2	2.8056(51)	2.6761(35)
Angles(°)	P1-Ag1-P2	112.63(6)	117.67(4)
	P2-Ag1- N1	139.22(15)	106.21(9)
	N1-Ag1-P1	106.56(14)	133.88(9)

7. Computational Methodology and Results

The distribution of frontier molecule orbitals and excited states were obtained from the Gaussian 09 program [2]. The density functional theory (DFT) and time-dependent (TD-DFT) density functional theory calculations were performed at PBE0 level using 6-31g*/LANL2DZ basis sets in conjunction with the polarizable continuum model (PCM) using dichloromethane as the solvent. The structures in the singlet ground (S_0) state were optimized via DFT. The S1 and T1 geometries were optimized via TDDFT. The input coordinates were extracted from the X-ray crystallographic data. Charge density differences (CDD) upon the $S_0 \rightarrow S_1$ and $S_0 \rightarrow$Tn transitions were carried out using Multiwfn 3.7 program [3]. The computational results of compound spiro-2N reference to the literature [1].

Table S3. The singlet (S_1) and triplet (T_n) states transition configurations of **1** calculated by TD-DFT based on optimized S_0 geometry.

	Orbs	Energy (eV)	Transition Configuration
S_n	1	2.8531	H→L(99.38%)
T_n	1	2.8432	H→L(98.76%)
	2	3.0211	H-2→L(46.04%), H-2→L+1(15.19%), H-13→L(12.36%), H-16→L(10.33%), H-25→L+21(2.65%), H-23→L(2.63%), H-22→L+3(2.26%), H-13→L+1(1.83%), H-23→L+1(1.30%), H-16→L+1(1.10%)
	3	3.1005	H→L+3(34.59%), H→L+16(15.55%), H→L+17(8.53%), H→L+11(7.39%), H-2→L+9(4.74%), H-5→L+19(4.46%), H-6→L+23(3.19%), H→L+15(2.32%), H→L+21(2.23%), H→L+1(2.12%), H-13→L+23(2.08%), H-5→L+11(2.01%), H→L+4(1.95%), H-16→L+9(1.91%)

Table S4. The singlet (S_1) and triplet (T_n) states transition configurations of **2** calculated by TD-DFT based on optimized S_0 geometry.

	Orbs	Energy (eV)	Transition Configuration
S_n	1	2.8514	H→L(99.35%)
T_n	1	2.8384	H→L(98.36%)
	2	3.0211	H-3→L(45.68%), H-3→L+1(15.30%), H-12→L(13.67%), H-17→L(9.81%), H-23→L(2.82%), H-25→L+21(2.74%), H-22→L+3(2.41%), H-12→L+1(2.04%), H-23→L+1(1.32%), H-17→L+1(1.09%)
	3	3.0999	H→L+3(32.77%), H→L+15(24.46%), H→L+1(7.05%), H→L+11(6.95%), H-3→L+9(5.15%), H-5→L+19(4.29%), H-7→L+23(3.01%), H→L+21(2.27%), H-17→L+9(2.08%), H-12→L+23(2.03%), H-5→L+11(1.75%), H→L+14(1.44%)

1	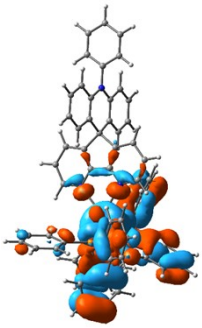	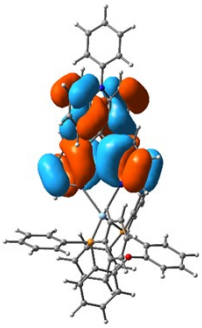	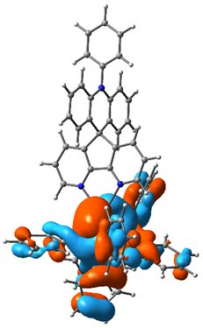	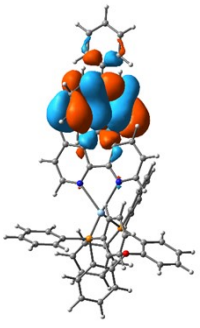
	HOMO-3	HOMO-2	HOMO-1	HOMO
	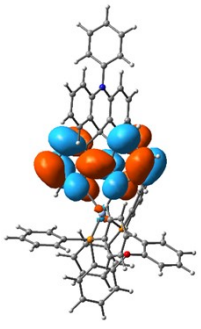	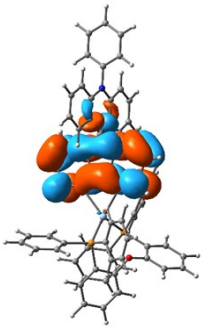	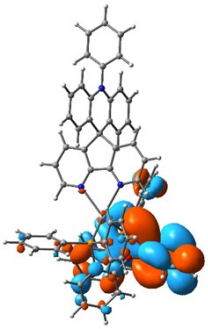	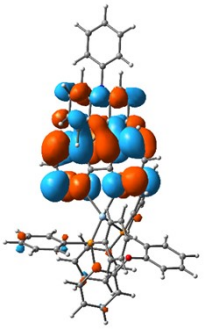
	LUMO	LUMO+1	LUMO+2	LUMO+3
2	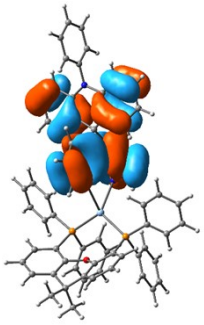	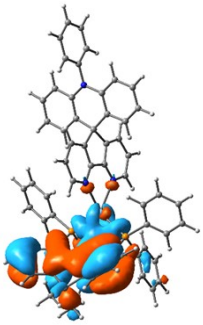	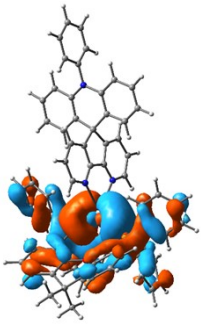	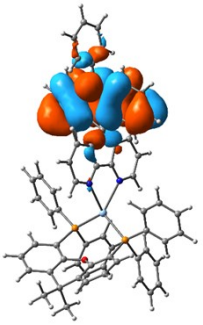
	HOMO-3	HOMO-2	HOMO-1	HOMO
	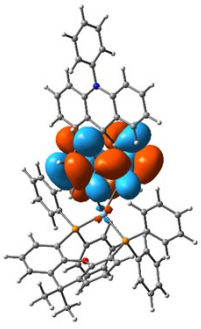	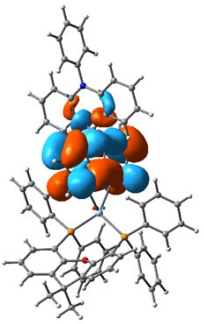	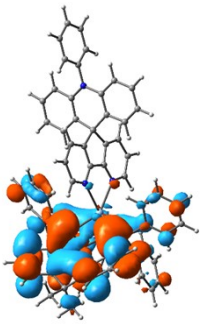	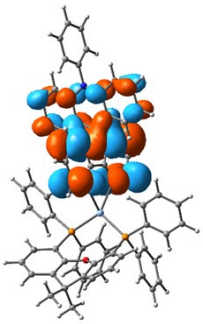
	LUMO	LUMO+1	LUMO+2	LUMO+3

Fig. S8. The electronic density contour of complex **1** and **2**.

	1		2	
	Electron	Hole	Electron	hole
S_1	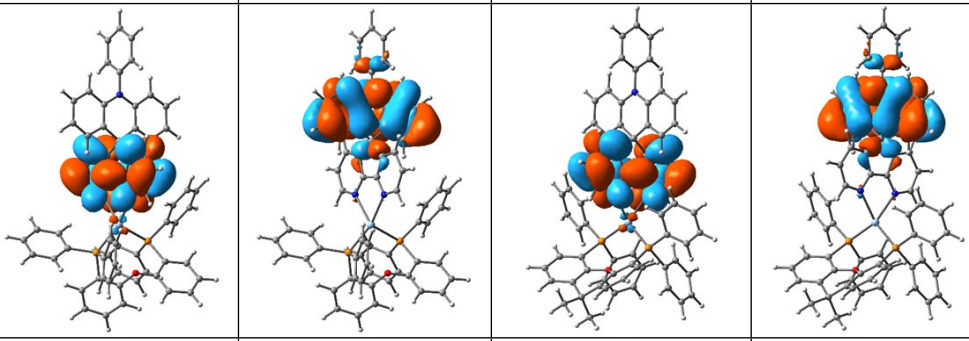			
T_1	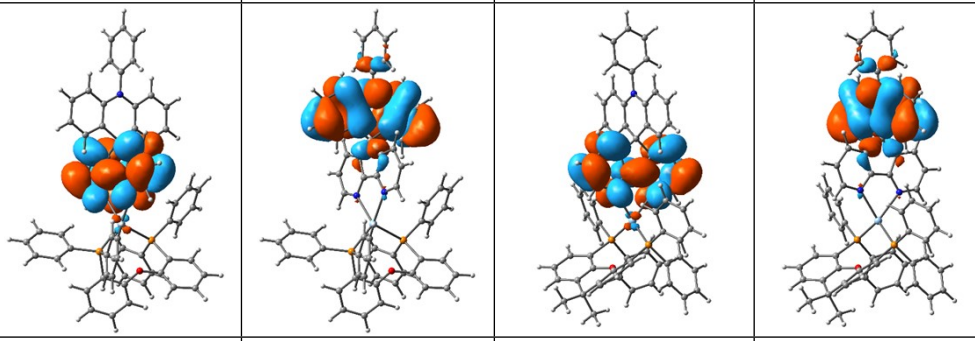			

Fig. S9. The electronic density contour of isolated and coupled on optimized S_1 and T_1 structure.

	1		2	
	Electron	Hole	Electron	hole
S_1	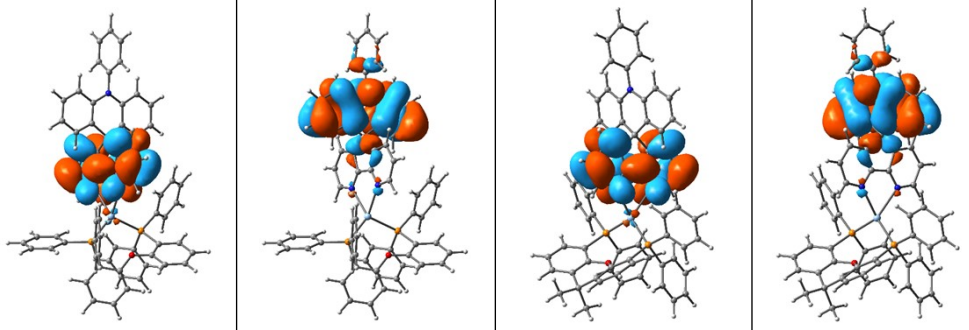			
T_1	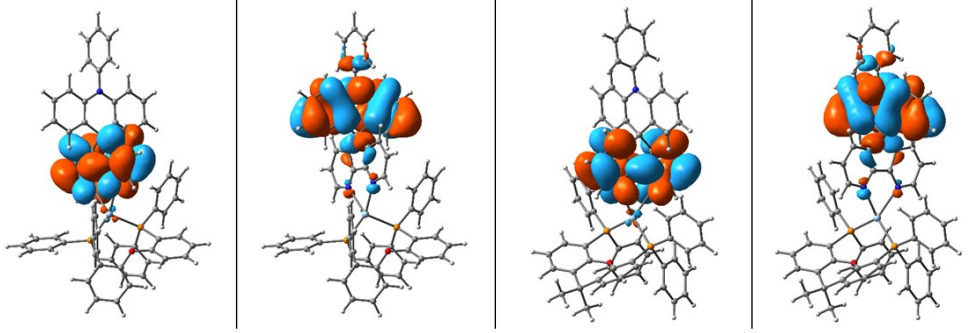			

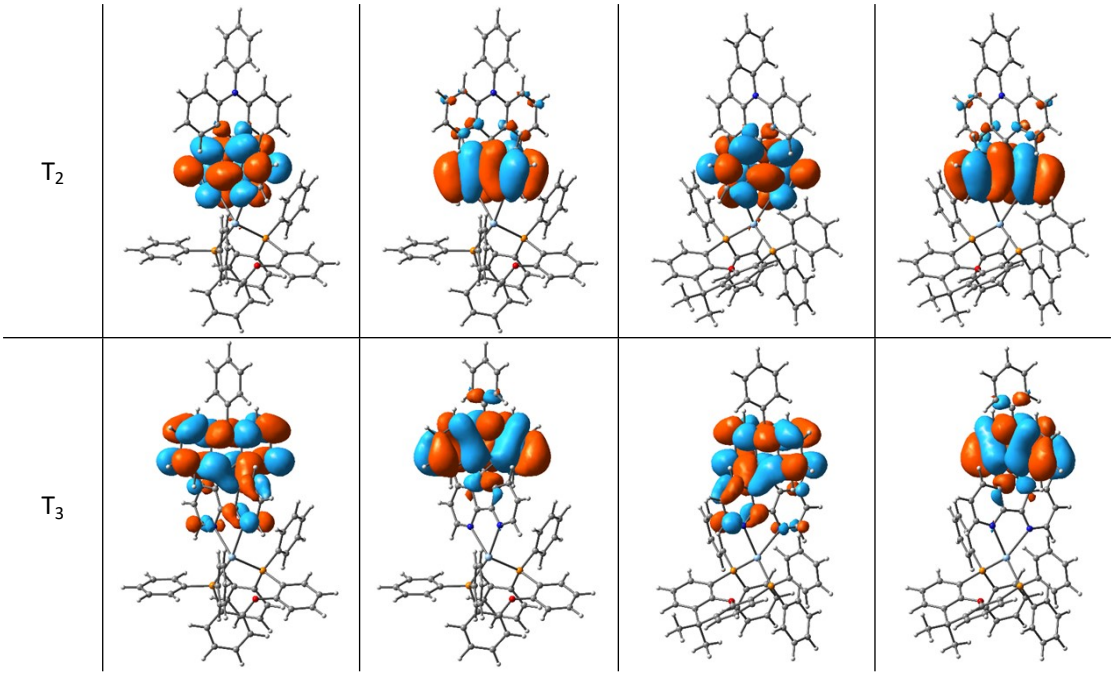

Fig. S10. The electronic density contour of isolated and coupled on optimized S_0 structure.

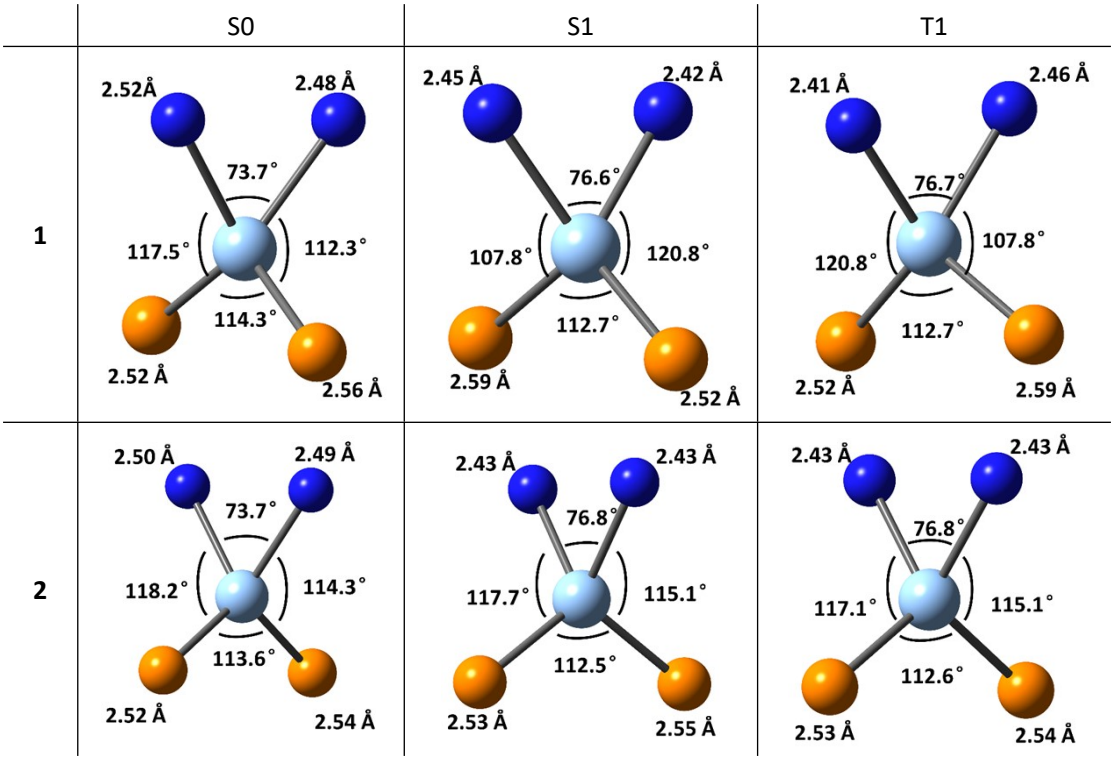

Fig. S11. Coordination geometries structures of **1** and **2** in S_0, S_1, and T_1 states optimized with DFT and TD-DFT.

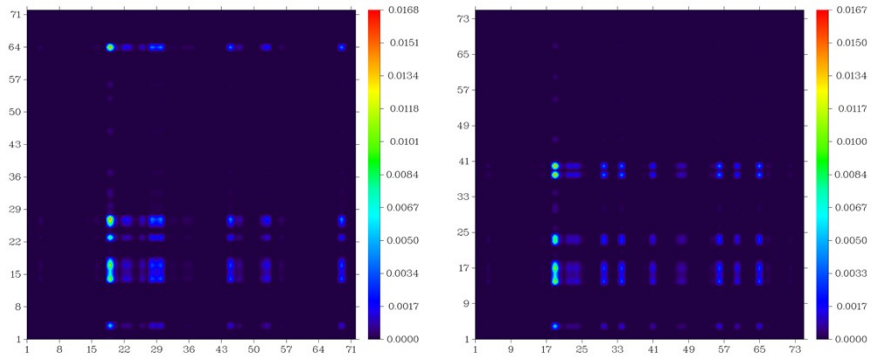

Fig. S12 The transition density matrix of complex **1** (left) and **2** (right).

8. Photophysical Properties

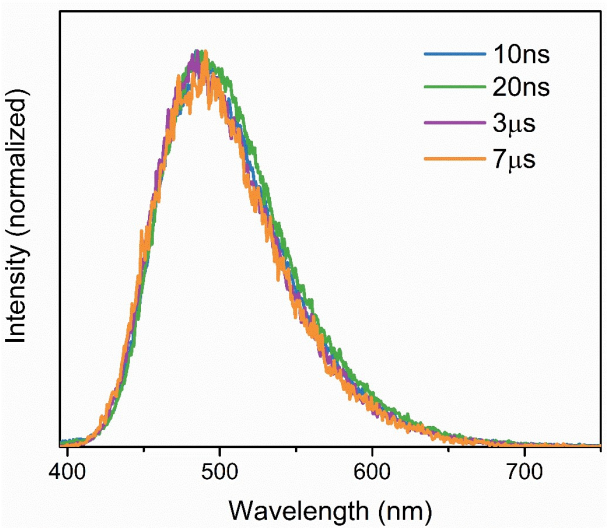

Fig. S13. Time-resolved PL spectra of **1** in 10wt%-doped PMMA film at 298K.

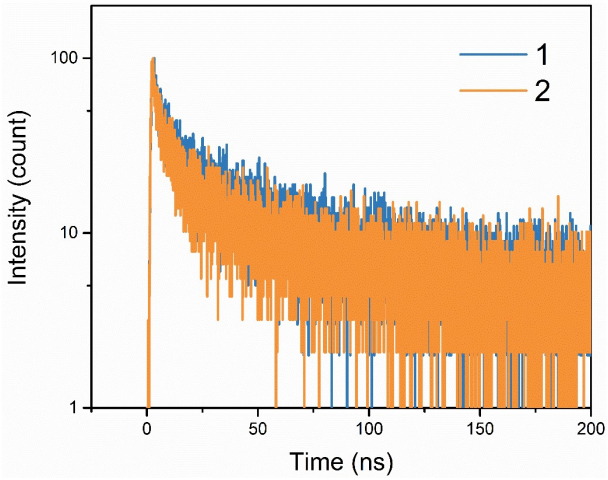

Fig. S14. Transient PL decay spectrum of **1** and **2** doped into PMMA films (10 wt%) at 298K.

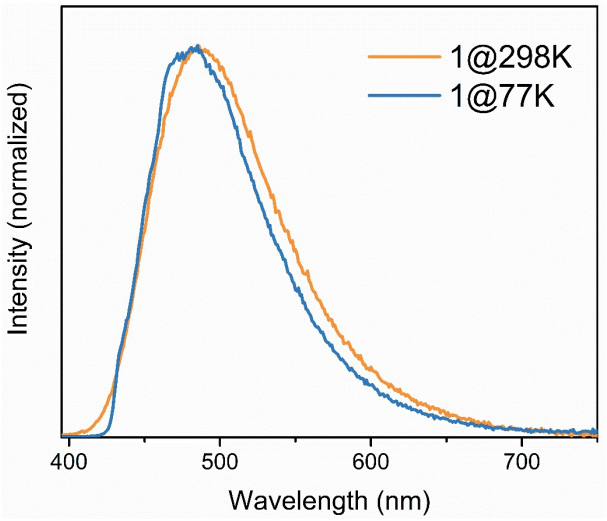

Fig. S15. PL spectra of complexes **1** doped in PMMA film (10 wt%) at 298K and 77K.

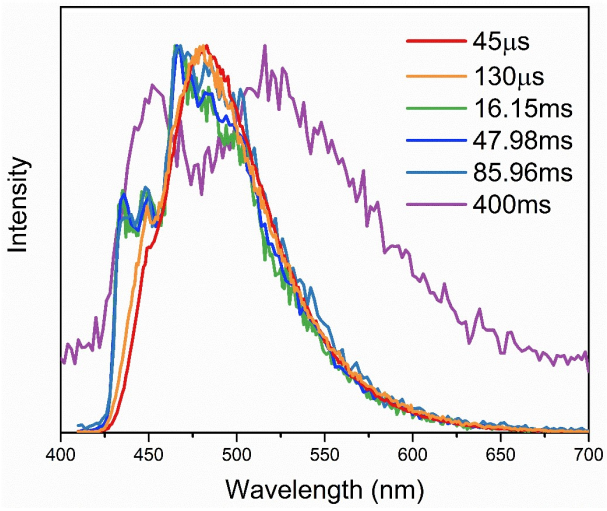

Fig. S16. Time-resolved PL spectra of **1** in 10wt%-doped PMMA film at 77K.

9. Equations

According to Fermi's golden rule, the ISC rate can be described as follow [4]:

$$k_{ISC} \propto \langle {}^3\Psi | \hat{H}_{SO} | {}^1\Psi \rangle / exp(\Delta E_{ST}^2) \quad (1)$$

The rate of ISC, RISC, radiative rate constant (k_r^S) can be calculated from the experimental data as follow [5-8]:

$$k_P = \frac{1}{\tau_P} \quad (2)$$

$$k_d = \frac{1}{\tau_d} \quad (3)$$

$$k_r^S = \Phi_F k_P \quad (4)$$

$$k_{ISC} = \left(1 - \frac{\Phi_F}{\Phi}\right) k_P \quad (5)$$

$$k_{RISC} = \frac{k_P k_d \Phi_{TADF}}{k_{ISC} \Phi_F} \quad (6)$$

Where τ_P is the transient decay time of the prompt component, τ_d is the transient decay time of the delayed component, ΦF and ΦTADF are the prompt and delayed components of the PL quantum efficiency, respectively.

10. Reference

1 Liang D, Jia J-H, Yang M, et al. *Adv Opt Mater*, 2022: 2201130, doi:10.1002/adom.202201130

2 M. J. Frisch, G. W. Trucks, H. B. Schlegel, G. E. Scuseria, M. A. Robb, J. R. Cheeseman, G. Scalmani, V. Barone, B. Mennucci, G. A. Petersson, H. Nakatsuji, M. Caricato, X. Li, H. P. Hratchian, A. F. Izmaylov, J. Bloino, G. Zheng, J. L. Sonnenberg, M. Hada, M. Ehara, K. Toyota, R. Fukuda, J. Hasegawa, M. Ishida, T. Nakajima, Y. Honda, O. Kitao, H. Nakai, T. Vreven, J. A. Montgomery, J. E. P. Jr., F. Ogliaro, M. Bearpark, J. J. Heyd, E. Brothers, K. N. Kudin, V. N. Staroverov, R. Kobayashi, J. Normand, K. Raghavachari, A. Rendell, J. C. Burant, S. S. Iyengar, J. Tomasi, M. Cossi, N. Rega, J. M. Millam, M. Klene, J. E. Knox, J. B. Cross, V. Bakken, C. Adamo, J. Jaramillo, R. Gomperts, R. E. Stratmann, O. Yazyev, A. J. Austin, R. Cammi, C. Pomelli, J. W. Ochterski, R. L. Martin, K. Morokuma, V. G. Zakrzewski, G. A. Voth, P. Salvador, J. J. Dannenberg, S. Dapprich, A. D. Daniels, Ö. Farkas, J. B. Foresman, J. V. Ortiz, J. Cioslowski, D. J. Fox, Gaussian09, Revision D.01; Gaussian Inc.: Wallingford CT, **2016**

3 T. Lu, F. Chen, *J Comput Chem* **2012**, *33*, 580-592

4 Y. Xiong, Z. Zhao, W. Zhao, H. Ma, Q. Peng, Z. He, et al., *Angew Chem Int Ed, 2018, 57: 7997-8001*

5 L.-S. Cui, A. J. Gillett, S.-F. Zhang, H. Ye, Y. Liu, X.-K. Chen, Z.-S. Lin, E. W. Evans, W. K. Myers, T. K. Ronson, H. Nakanotani, S. Reineke, J.-L. Bredas, C. Adachi and R. H. Friend, Fast spin-flip enables efficient and stable organic electroluminescence from charge-transfer states, *Nat. Photonics*, 2020, **14**, 636-642.

6 K. Wang, W. Liu, C.-J. Zheng, Y.-Z. Shi, K. Liang, M. Zhang, X.-M. Ou and X.-H. Zhang, A comparative study of carbazole-based thermally activated delayed fluorescence emitters with different steric hindrance, *J. Mater. Chem. C*, 2017, **5**, 4797-4803.

7 D. Chen, X. Cai, X.-L. Li, Z. He, C. Cai, D. Chen and S.-J. Su, Efficient solution-processed red all-fluorescent organic light-emitting diodes employing thermally activated delayed fluorescence materials as assistant hosts: molecular design strategy and exciton dynamic analysis, *J. Mater. Chem. C*, 2017, **5**, 5223-5231.

8 Z. Cheng, J. Liang, Z. Li, T. Yang, C. Lin, X. Mu and Y. Wang, Photoluminescent manipulation of phenoxazine-based molecules via regulating conformational isomerization, and the corresponding electroluminescent properties, *J. Mater. Chem. C*, 2019, **7**, 14255-14263.